



HAL
open science

[68Ga]RGD Versus [18F]FDG PET Imaging in Monitoring Treatment Response of a Mouse Model of Human Glioblastoma Tumor with Bevacizumab and/or Temozolomide

Claire Provost, Laura Rozenblum-Beddok, Valérie Nataf, Fatiha Merabtene, Aurélie Prignon, Jean-Noël Talbot

► To cite this version:

Claire Provost, Laura Rozenblum-Beddok, Valérie Nataf, Fatiha Merabtene, Aurélie Prignon, et al.. [68Ga]RGD Versus [18F]FDG PET Imaging in Monitoring Treatment Response of a Mouse Model of Human Glioblastoma Tumor with Bevacizumab and/or Temozolomide. *Molecular Imaging and Biology*, 2019, 21 (2), pp.297-305. 10.1007/s11307-018-1224-9. hal-04028702

HAL Id: hal-04028702

<https://hal.science/hal-04028702>

Submitted on 21 Apr 2023

HAL is a multi-disciplinary open access archive for the deposit and dissemination of scientific research documents, whether they are published or not. The documents may come from teaching and research institutions in France or abroad, or from public or private research centers.

L'archive ouverte pluridisciplinaire **HAL**, est destinée au dépôt et à la diffusion de documents scientifiques de niveau recherche, publiés ou non, émanant des établissements d'enseignement et de recherche français ou étrangers, des laboratoires publics ou privés.

$[^{68}\text{Ga}]$ RGD Versus $[^{18}\text{F}]$ FDG PET Imaging in Monitoring Treatment Response of a Mouse Model of Human Glioblastoma Tumor with Bevacizumab and/or Temozolomide

Claire Provost ¹, Laura Rozenblum-Beddok,^{1,2} Valérie Nataf,^{1,2} Fatiha Merabtene,³ Aurélie Prignon,¹ Jean-Noël Talbot^{1,2}

¹Laboratoire d'Imagerie Moléculaire Positronique (LIMP), UMS 28, UPMC - Sorbonne Universités, Paris, France

²Service de Médecine Nucléaire et Radiopharmacie, Hôpital Tenon, AP-HP, Paris, France

³Plateforme d'Histomorphologie Service d'Anatomie Pathologique, Hôpital Saint Antoine, AP-HP, Paris, France

Abstract

Purpose: The aim of this study was to evaluate positron emission tomography (PET) imaging with $[^{68}\text{Ga}]$ NODAGA-c(RGDfK) ($[^{68}\text{Ga}]$ RGD), in comparison with 2-deoxy-2- $[^{18}\text{F}]$ fluoro-D-glucose ($[^{18}\text{F}]$ FDG), for early monitoring of the efficacy of an antiangiogenic agent associated or not with chemotherapy, in a mouse model of glioblastoma (GB).

Procedures: Mice bearing U87MG human GB cells line were parted into five groups of five mice each. One group was imaged at baseline before the treatment phase; another group was treated with bevacizumab (BVZ), another group with temozolomide (TMZ), another group with both agents, and the last one was the control group. Tumors growth and biological properties were evaluated by caliper measurements and PET imaging at three time points (baseline, during treatment t1 = 4–6 days and t2 = 10–12 days). At the end of the study, tumors were counted and analyzed by immunohistochemistry (CD31 to evaluate microvessel density).

Results: The tumor volume assessed by caliper measurements was significantly greater at t1 in the control group than in the TMZ + BVZ-treated group or in the BVZ-treated group. At t2, tumor volume of all treated groups was significantly smaller than that of the control group. $[^{18}\text{F}]$ FDG PET failed to reflect this efficacy of treatment. In contrast, at t1, the $[^{68}\text{Ga}]$ RGD tumor uptake was concordant with tumor growth in controls and in treated groups. At t2, a significant increase in tumor uptake of $[^{68}\text{Ga}]$ RGD vs. t1 was only observed in the TMZ-treated group, reflecting a lack of angiogenesis inhibition, whereas TMZ + BVZ resulted in a dramatic tumor arrest, reduction in microvessel density and stable tumor $[^{68}\text{Ga}]$ RGD uptake.

Conclusions: $[^{68}\text{Ga}]$ RGD is a useful PET agent for *in vivo* angiogenesis imaging and can be useful for monitoring antiangiogenic treatment associated or not with chemotherapy.

Key words: PET, Integrins $\alpha\beta_3$, Angiogenesis, $[^{68}\text{Ga}]$ RGD, $[^{18}\text{F}]$ FDG, Bevacizumab, Temozolomide

Introduction

Angiogenesis is currently the object of a high interest, in particular because of its significant role in several common diseases [1] and for drug targeting [2–4]. As a result, antiangiogenic drugs have emerged to expand the resources for cancer treatment, in particular bevacizumab (BVZ) [5–7]. However, even in cancers with high vasculature proliferation, not all the patients can benefit from a specific antiangiogenic therapy as some patients do not respond [8–10]. The radioactive glucose analogue 2-deoxy-2-[¹⁸F]fluoro-D-glucose ([¹⁸F]FDG), the most common radiotracer in oncologic positron emission tomography (PET), have been used for predicting survival following antiangiogenic therapy in different cancers. Colavolpe, et al. [11] performed brain FDG PET in 25 patients with recurrent high-grade gliomas, within 6 weeks of starting bevacizumab and irinotecan chemotherapy. Tumor [¹⁸F]FDG uptake significantly predicted PFS and OS. In multivariate analysis, the tumor SUVmax and its ratio to the contralateral site were the most powerful independent predictors of PFS and OS. Sensitivity and specificity for predicting death at 6 months were respectively 88 and 59 %. In preclinical studies, results are conflicted, the [¹⁸F]FDG potential for monitoring an early response to antiangiogenic seems to depend on the agent [12–14]. Another interesting marker aiming to predict an effect of antiangiogenic therapy is the overexpression of integrin $\alpha\beta3$, a heterodimeric transmembrane glycoprotein, which mediates cell-matrix and cell-cell interactions. Integrin $\alpha\beta3$ is overexpressed in activated endothelial cells, where it plays a critical role in the angiogenic process. Moreover, studies have shown that $\alpha\beta3$ is an important receptor affecting tumor growth, local invasiveness, and metastatic potential [15, 16]. A part of natural ligands of integrin $\alpha\beta3$ has been identified, notably an important binding epitope, the amino-acid sequence arginine-glycine-aspartic acid (RGD). For diagnostic imaging, various positron emission tomography (PET) tracers incorporating the RGD sequence have been developed and radiolabeled with different radionuclides [17]. Clinical studies on rather small series have shown the potential of dimeric RGD peptide tracers, such as [¹⁸F]FPPRGD2 and alfatide for detecting cancer extension [18]. Tumor response to antiangiogenic therapy has also been studied: Zhang, et al. performed a pilot clinical study in patients with glioma using [¹⁸F]AIF-NOTA-PRGD2 (alfatide II) and highlighted the potential of semi-quantification (mainly with SUVmax) of PET performed either before or after 3 weeks of treatment to predict tumor response to concurrent chemoradiotherapy. SUVmax values decreased from baseline to treatment PETs, 1.37 ± 0.40 vs. 1.03 ± 0.40 ($P < 0.05$) in the responder group, whereas no significant change was noted in the non-responder group (SUVmax 2.14 ± 1.00 vs. 2.19 ± 1.12 , $P > 0.05$) [19]. Likewise, Iagaru et al. performed a prospective trial to evaluate [¹⁸F]FPPRGD2 PET in patients with glioblastoma multiforme (GBM) treated with BVZ. In this

study, the decrease of [¹⁸F]FPPRGD2 uptake, just 1 week after BVZ administration, was a predictor of therapy outcome. The SUVmax values decreased between baseline and after 1 week of treatment ($P = 0.025$) and was not significantly modified later [20].

To further investigate the potential of RGD imaging, preclinical studies using several radiolabeled RGD peptides for PET imaging were performed on the experimental U87MG model of human glioblastoma (GB). The U87MG cell line overexpresses the integrin $\alpha\beta3$ and is very aggressive and highly vascularized [21]. Some recent preclinical studies addressed the ability of the RGD PET radiotracers to monitor antiangiogenic treatment [12, 22–25]. Battle, et al., in an animal model of GB, showed a decrease in tumor uptake of [¹⁸F]AH111585 (or fluciclatide) after antiangiogenic (sunitinib) therapy, before observing a reduction in tumor volume [26]. Most of the RGD radioligands have been radiolabeled with F-18. RGD ligands radiolabeled with Ga-68 have been introduced more recently [27, 28]. It is true that the energy of the beta + particle of Ga-68 is greater, leading to some loss of resolution in the PET images. In contrast, labeling with Ga-68 has some advantages. Thanks to the ⁶⁸Ge/⁶⁸Ga generator, the labeling of tracer lyophilized RGD tracer is feasible at any moment in the radiopharmacy. Thus, urgent pretreatment PET/CT may be performed, independently of the delivery of a F-18 labeled ligand by an industrial firm, when the PET center has no on-site cyclotron. Furthermore, the Ga-68 atom may be substituted in the chelate by a radionuclide for internal radiotherapy (e.g., Lu-177), which is not the case for the F-18 labeled radiotracers. The ligand [⁶⁸Ga]NODAGA-c(RGDfK) used in the present study (and referred as [⁶⁸Ga]RGD in this article) was described by Knetsch in 2011 [29] and was recently tried in humans [30].

The aim of the present study was to evaluate this Ga-68 labeled RGD radiotracer, in comparison with [¹⁸F]FDG, for monitoring the early therapeutic response to an antiangiogenic agent, BVZ, associated or not with temozolomide (TMZ) chemotherapy, in a mouse model grafted with human GB.

Materials and Methods

Radiolabeling

The radiolabeling of NODAGA-c(RGDfK) with Ga-68 was already described [31]. Quality control was performed using high-performance liquid chromatography (HPLC) combined with a Berthold radio-HPLC detector. The HPLC mobile phase A was a mixture of water with 0.1 % of trifluoroacetic acid (TFA) and phase B, acetonitrile with 0.1 % of TFA. The HPLC Reverse Phase C18 column (Symmetry C18, 5 μ m, Waters) flow rate was 1 ml/min. Column was equilibrated with 100% A; the HPLC gradient was 0–55 % B over 15 min, (flow 1 ml/min). Retention time was around 10 min at 30 % of B.

Animal Model

U87MG human GB cells lines were maintained in RPMI 1640 with L-Glutamine (Sigma-Aldrich) supplemented with 10 % fetal calf serum and 1 % penicillin/streptomycin (Sigma-Aldrich). Cells were grown in T175 CellBind flasks (CellBind Flask Sigma-Aldrich) at 37 °C in a humidified atmosphere containing 5 % CO₂.

Twenty-five Swiss female nude mice aged 6 weeks (Charles River) received subcutaneous grafts in right back leg by injection of 3×10^6 cells suspended in 100 µl of phosphate buffered saline (PBS) and mixed 50/50 with Matrigel (BD Biosciences). Tumor volumes were measured twice a week with a caliper. The volumes were calculated from the two perpendicular diameters using the formula: $V = \pi/6 * l * w^2$, in which l = length and w = width. Volume was expressed as mean \pm SD in cubic millimeters. Five of these five mice were used to determine baseline SUVmax values before the treatments. All animal experiments were carried out in compliance with the French laws relating to the conduct of animal experimentation, in application of the directive 2010/63/EU.

Treatment

For treatment monitoring, 20 mice were parted into 4 homogeneous groups of 5 mice. All treatments were injected intraperitoneally (IP), twice a week during 2 weeks (Fig. 1). The first group was injected 17 mg/kg of TMZ, the second one with 20 mg/kg of BVZ, the third one with 20 mg/kg of BVZ, and 17 mg/kg of TMZ at the same time and the control group with PBS.

PET Imaging

PET acquisitions were obtained using the Mosaic animal PET machine (Philips Medical systems, Cleveland, OH, USA). Before [¹⁸F]FDG PET imaging, mice were fasted for 7 h with free access to water; for the [⁶⁸Ga]RGD tracer imaging, animals were not fasted. Around 5 MBq of

[¹⁸F]FDG or around 1.6 MBq (~600 pmol) of [⁶⁸Ga]RGD were injected intravenously in the retro-orbital sinus. Static PET acquisitions were obtained over 10 min starting 1 h after [¹⁸F]FDG injection or 40 min after [⁶⁸Ga]RGD injection. Mice were maintained under 1.5 % isoflurane anesthesia during image acquisition. After acquisition, images were reconstructed and visualized either as maximum intensity projection (MIP) or as slices (sagittal, transverse, coronal) for visual and quantitative analysis. Regions of interest (ROI) were drawn manually around the tumor, using a Syntegra–Philips software (PETView; Philips Medical Systems). The uptake was quantified as maximum standardized uptake value (SUVmax), which corresponds to the maximal radioactivity concentration in the pixels of the ROI (kBq/ml) multiplied by body mass (g) and divided by injected radioactivity (kBq).

Study Design

The schedule of study is summarized in Fig. 1. After the xenograft of 25 mice, the first PET imaging for baseline, when the tumor volume reached around 300 mm³, was performed into five mice with [¹⁸F]FDG and 48 h later with [⁶⁸Ga]RGD. To evidence the viability and metabolic activity of the tumors before starting the treatment, five grafted mice were imaged with [¹⁸F]FDG, and 48 h later with [⁶⁸Ga]RGD, to be sure that their tumor took up these tracers at baseline. The mice of this “baseline” group were kept alive to replace mice that died in control group, but they were actually not further imaged. The 20 mice remaining were randomized into four groups ($n=5$ per group). Treatments began at day 25 when tumor volume reached around 450 mm³. The 2nd PET imaging (t1) was performed after two injections of the therapy, 4–6 days after the beginning of treatment. [¹⁸F]FDG PET was performed first and [⁶⁸Ga]RGD PET 48 h later. The 3rd PET imaging (t2) was performed similarly after four injections of the therapy, 10–12 days after the beginning of treatment (Fig. 1).

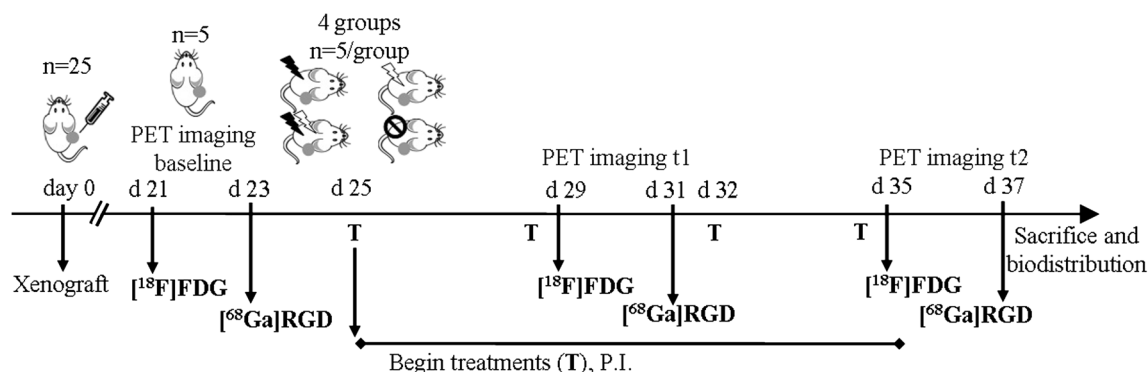


Fig. 1. Experimental study design for monitoring treatment efficacy with [⁶⁸Ga]RGD and [¹⁸F]FDG. T: intraperitoneal administration of treatment. Four groups: TMZ treated, BVZ treated, TMZ + BVZ treated, controls.

Ex vivo Biodistribution

One hour after the last injection of [⁶⁸Ga]RGD followed by PET imaging, mice were euthanized and dissected. Tumors were removed, weighed, and counted in a gamma-counter (1480 Wizard 3, Perkin Elmer). Tumor uptake was expressed as mean \pm SD percentage of injected activity of tissue (%ID) and corrected for Ga-68 decay.

Immunohistochemistry

All tumors were embedded in paraffin according to standard procedures and different staining were performed: hematoxylin-eosin (HE) for evaluating tissue appearance and an antimouse CD31 antibody (Abcam, UK) was used to evaluate the relative microvessel density (MVD) (%) \pm SD expression. The tumor slices were observed with an optical microscope in transmitted light, at $\times 20$ magnification (Nikon Eclipse, Champigny sur Marne, France). Quantitative analysis of the immunostaining was performed by evaluating the percentage of positive area within the area of the entire section, using an Image J software.

Statistical Analysis

Caliper volume measurements and SUVmax values were expressed as mean \pm SD. One-way ANOVA followed by Tukey's post-hoc test or two-way ANOVA was used to search for differences between groups. Paired samples *t* test was used to search in each group for significant variations between results at t1 and t2. The statistical analysis was performed with a GraphPad software (USA).

Results

Radiolabelling

The overall decay-corrected radiochemical yield (RY) was 98 %; the radiochemical purity was ≥ 98 % using analytical HPLC, and the specific radioactivity (SR) was 5.5 and 5.8 MBq/nmol ($n = 2$).

Effect of Treatments on Tumor Growth

Figure 2 and Table 1 illustrate the evolution of tumor volume evaluated by means of caliper in each group of mice. We performed a two-way ANOVA, the 1st factor was about time, and consisting in five dates of tumor measurement (Fig. 2). The 2nd factor was the treatment (PBS for the control group). The 1st, the 2nd, and the interaction between both factors had a significant effect on tumor volume ($P < 0.0001$). Tumor growth was significantly faster in controls than in all other groups ($P < 0.0001$) and in TMZ or BVZ alone vs. TMZ + BVZ ($P = 0.007$ for TMZ and $P =$

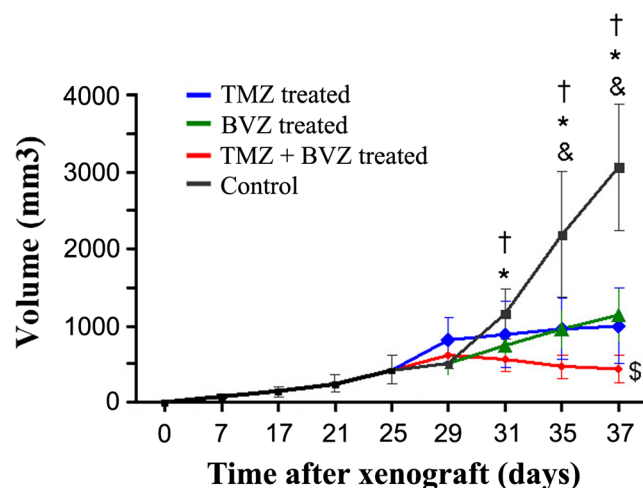


Fig. 2. **a** Follow-up of tumor volume, measured with caliper, of 20 mice grafted with U87MG cells. Blue curve, TMZ-treated mice; green curve, BVZ-treated mice; red curve, TMZ + BVZ treated; black curve, controls ($n = 5$ per group). ($P < 0.05$, controls vs. BVZ treated indicated by a single asterisk, vs. TMZ + BVZ treated indicated by a single dagger, vs. TMZ treated indicated by an single ampersand, and TMZ + BVZ treated vs. BVZ treated indicated by a single dollar sign). **b** Mean increase in tumor volume between d25 and d35 for each group.

0.05 for BVZ), the only regimen that resulted in a decrease in tumor size.

Thirty-one days after xenograft and 6 days after the beginning of treatment, tumor volume was significantly larger in the control group than in the TMZ + BVZ-treated group and in the BVZ-treated group ($P < 0.05$). Thirty-five days after xenograft and 10 days after the beginning of treatment, tumor volume was significantly larger in controls than in all treated groups ($P < 0.05$), and this difference was reinforced on day 37, 12 days after the beginning of treatment ($P < 0.05$).

Evaluation of the Effect of Treatment with [¹⁸F]FDG PET

At baseline, the mean tumor of [¹⁸F]FDG SUVmax was no significantly different than the mean tumor of [¹⁸F]FDG SUVmax in each group at t1 and at t2. In the first and second PET imaging sessions, there was no significant difference in mean [¹⁸F]FDG SUVmax between the four

Table 1. Quantitative changes in tumor volume

Groups	Mean increase between d25 and d37
TMZ	140 %
BVZ	170 %
TMZ + BVZ	5 %
Control	630 %

groups. No difference in mean [^{18}F]FDG SUVmax was observed between t1 and t2 for any group (Fig. 3a). In the control group, a photopenic zone was observed at t2 in the center of all the tumors (rim sign) reflecting a reduction in glucose metabolism (Fig. 3b), caused by tumor necrosis (Fig. 3c).

Evaluation of the Effect of Treatment with [^{68}Ga]RGD PET

At baseline, the mean tumor [^{68}Ga]RGD SUVmax was 1.00 ± 0.29 , uptake values in each other group at t1 or t2 compared to the baseline were no significantly different. At t1, the mean tumor [^{68}Ga]RGD SUVmax was significantly greater in the control group than in BVZ or TMZ + BVZ-treated mice; no difference was observed between controls and TMZ-treated group (Fig. 4a). However, the difference between controls and treated groups observed at t1 was no longer significant at t2. On the other hand, at t2, the mean tumor [^{68}Ga]RGD SUVmax in the TMZ-treated group was significantly greater than that of the BVZ-treated groups (Fig. 4a).

The mean SUVmax of control group decreased significantly between t1 and t2: 1.22 ± 0.27 at t1 vs. 0.90 ± 0.21 at t2. A significant increase in mean tumor uptake of [^{68}Ga]RGD was only observed in the TMZ-treated group: SUVmax was 0.92 ± 0.1 at t1 and 1.24 ± 0.2 at t2 ($P < 0.05$) (Fig. 4b).

Ex vivo tumor uptake of [^{68}Ga]RGD in treated groups was clearly higher when mice were treated with TMZ alone than with the two other treatments, 4.50 ± 1.33 % ID/g vs. 2.36 ± 0.53 % ID/g in BVZ-treated tumors and 2.07 ± 0.80 % ID/g in tumors treated with TMZ + BVZ ($P < 0.05$). Tumor [^{68}Ga]RGD uptake was low but no significantly different in TMZ-treated group than in the control group: 3.27 ± 0.85 %ID/g (Fig. 4c).

CD31-positive microvessels were detected in the tumors of the control group, with a percentage of positive area of 0.92 ± 0.79 %, similar to 0.92 ± 0.75 % in TMZ-treated tumors. In the other groups, MVD was low and few, microvessels could be detected. The percentage of positive area in tumors was 0.06 ± 0.05 % and 0.08 ± 0.06 % in the groups treated with BVZ or with TMZ + BVZ, respectively (Fig. 5).

Discussion

If one considers the rapid evolution of GB in humans and the high cost related to modern therapeutic regimens, it is important to monitor the efficiency of antiangiogenic agents, in order to discontinue ineffective treatments. Previous reports suggested PET imaging was an adequate technique for such monitoring [32]. Some preclinical and clinical studies used [^{18}F]FDG, but the results remain conflicting [14, 20, 33–35]. The objective of our study was to investigate the interest of [^{68}Ga]RGD, a PET marker of angiogenesis, compared to [^{18}F]FDG for monitoring an antiangiogenic treatment with BVZ and/or an alternative treatment with TMZ, in a mouse model of human GB. To the best of our knowledge, this is the first study which evaluated the effect of chemotherapy and/or antiangiogenic in a GB model by means of PET with a [^{68}Ga]RGD radiotracer.

Subcutaneous xenografting was chosen, since it enables to follow the evolution of the tumor volume by caliper measurements. From the first week, BVZ and BVZ + TMZ treatments induced a clearly significant reduction in the slope of tumor growth, as compared to controls. At the end of the second week, the tumor volume of all the treated mice was significantly smaller than that of the control group (Fig. 2). We observed that the tumor growth was stopped by using a combined TMZ + BVZ regimen; whereas, BVZ or

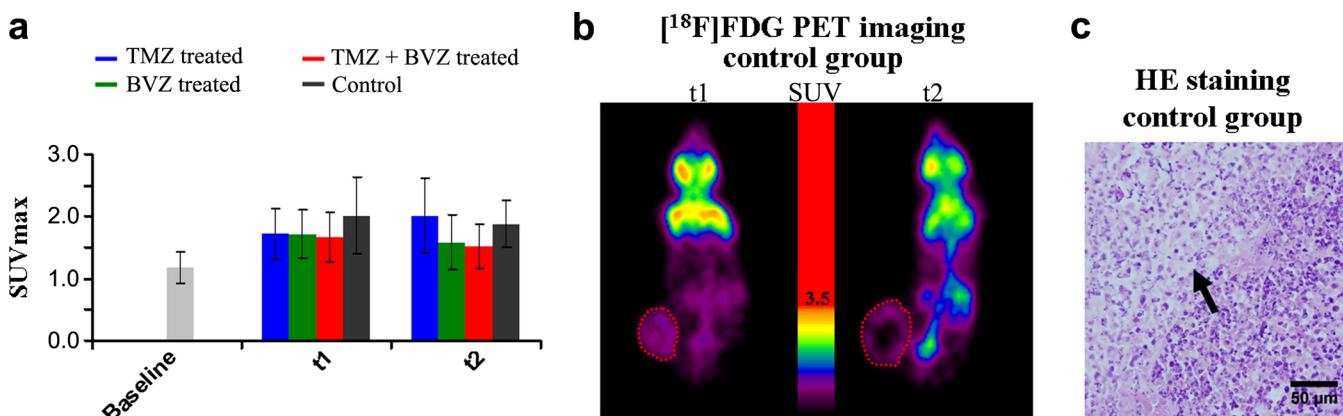


Fig. 3. **a** Quantitative [^{18}F]FDG SUVmax mean \pm SD in U87MG-tumor-bearing mice after 1 week (t1) or 2 weeks (t2) of treatment. Blue bars, TMZ treated; green bars, BVZ treated; red bars, TMZ + BVZ treated; black bars, controls ($n = 5$ per group). **b** Representative image of [^{18}F]FDG PET at t1 and t2 of a mouse from the control group, the tumors are surrounded by a red dotted line. **c** Representative slice of HE staining (same mouse tumor imaging PET), the black arrow points to the necrotic part of the tumor.

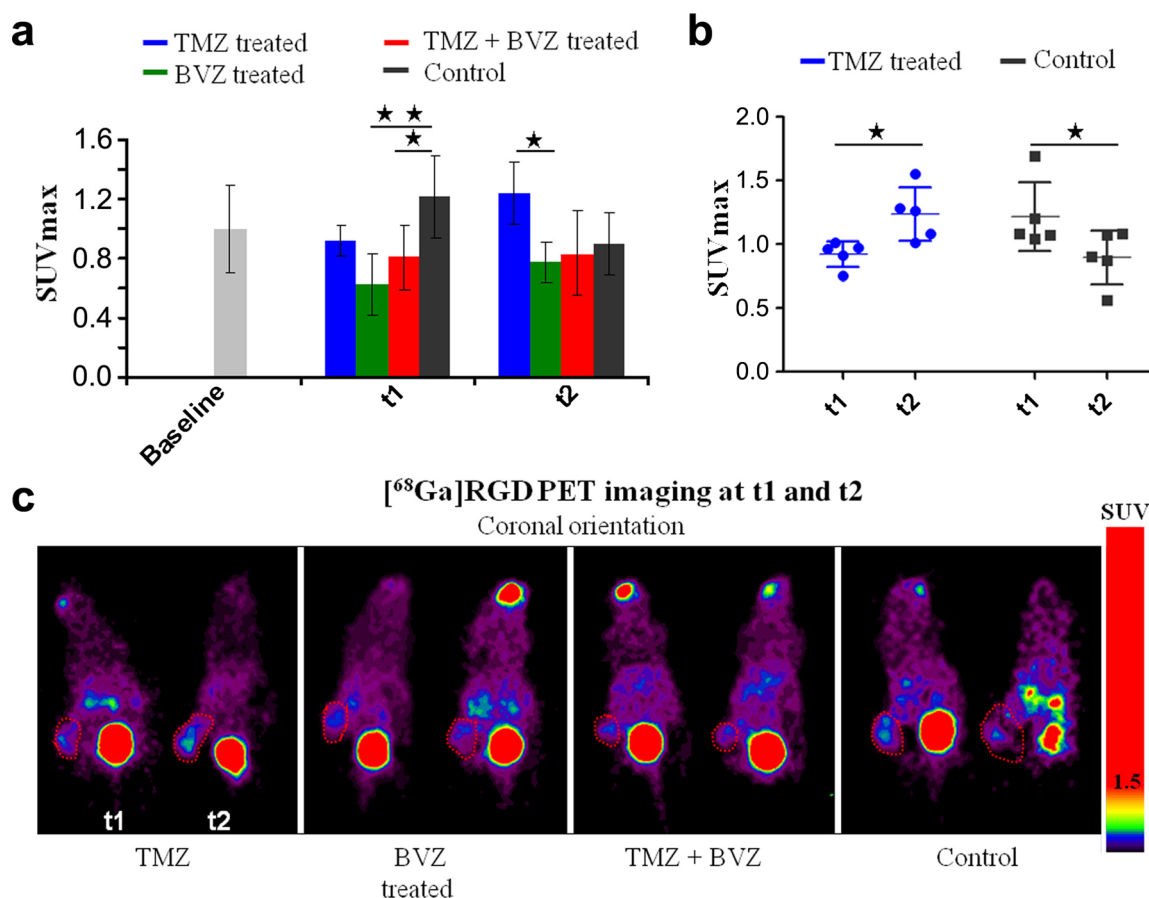


Fig. 4. [⁶⁸Ga]RGD PET results. **a, b** Quantitative [⁶⁸Ga]RGD SUVmax mean \pm SD of in U87MG-tumor-bearing mice after 1 week (t1) or 2 weeks (t2) of treatment. **c** Representative image of [⁶⁸Ga]RGD PET at t1 and t2 of a mouse from TMZ, BVZ, TMZ + BVZ-treated groups and control group, the tumors are surrounded by a red dotted line.

TMZ alone only resulted in a reduction of the slope of tumor growth. These results are explained by the mechanism of action of BVZ, which blocks vascular endothelial growth factor (VEGF-A). Therefore, it hampers tumor growth by mediating the regression of existing tumor vasculature and preventing regrowth over time [36, 37]. But this agent is not able to eradicate the tumor all by itself [38]. In the TMZ-treated group, chemotherapy created cytotoxic lesions resulting in an aberrant DNA repair leading to cell apoptosis. However, GB is known to be aggressive [39] and, as quoted in previous studies, U87MG GB model had a very fast tumor growth with a volume increase of more than 630 % in 2 weeks. The combination of those two agents appeared to be more efficient thanks to their synergic action on two different pathways that promote tumor growth. Similar results have been obtained by MRI measurement of tumor volume in an orthotopic rat model of human U87MG GB; after 2 weeks, the best response was induced by combined TMZ + BVZ treatment [34].

Even if [¹⁸F]FDG was taken up by U87MG tumors, the intensity of uptake was variable between tumors and did not correlate with the effect of treatment with BVZ or TMZ or a combination of both on the volume of GB tumors. Research

literature on the use of antiangiogenic treatments for U87MG model therapy gave conflicting results. One study reported that the [¹⁸F]FDG uptake in the tumor significantly increased after 13 days of the sunitinib treatment, whereas the tumor volume decreased [13]. Another team reported a substantial decrease in [¹⁸F]FDG uptake in U87MG tumor on day 10 after starting axitinib [12]. It is quite possible that each antiangiogenic drug has a different influence on the glucose transporter. Using the same treatment, similar results as ours were already reported by Corroyer-Dulmont et al. from an orthotopic rat U251 GB model [14]. Actually, [¹⁸F]FDG reflected the metabolic activity of untreated tumors of the control group at t1 and allowed to visually identify central necrosis at t2 (Fig. 3b, c), although the SUVmax value was not impacted.

At t1, a reduction in [⁶⁸Ga]RGD tumor uptake in comparison with controls was observed in the mice treated with BVZ alone or combined with TMZ, in agreement with a reduction in tumor growth. The interest of an early follow-up PET with a tracer RGD may be challenged, since MRI is able to visualize the evolution of the tumor volume as already shown [14]. However, our results show that [⁶⁸Ga]RGD PET may confirm the reduction in the angiogenic potential of the tumor when BVZ is used.

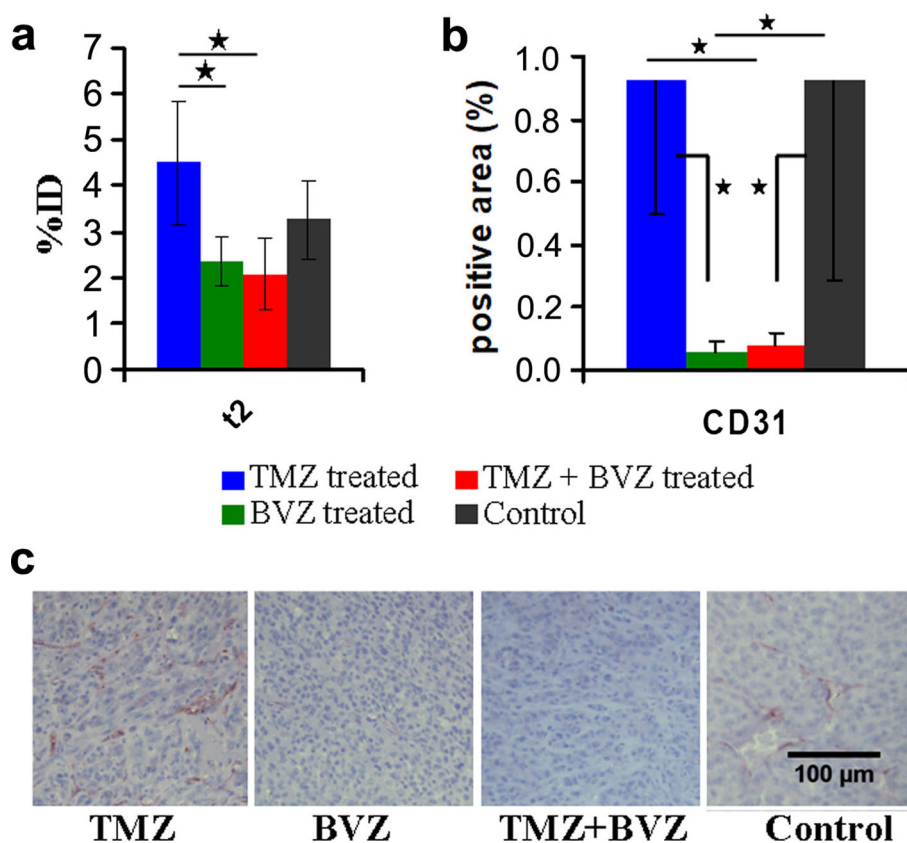


Fig. 5. **a** *Ex vivo* biodistribution of [^{68}Ga]RGD in tumor at t2, (%ID). Blue bar or dot, TMZ treated; green bar, BVZ treated; red bar, TMZ + BVZ treated; black bar or dot, control group ($n=5$ per group). $*p < 0.05$ and $**p < 0.005$. Immunohistochemistry staining CD31: **b** quantification by percentage of CD31-positive area in the tumor. Blue bars, TMZ treated; green bars, BVZ treated; red bars, TMZ + BVZ treated; black bars, control group ($n=5$ per group). $*p < 0.05$. **c** Representative images acquired at $\times 20$ magnification.

Between t1 and t2, the [^{68}Ga]RGD SUVmax increased significantly in the TMZ group, although the tumor volume only increased modestly (nonsignificant difference). SUVmax decreased in controls between t1 and t2 (Fig. 4b), whereas the tumor volume of which was definitely progressing. This decrease in [^{68}Ga]RGD uptake in controls could reflect the necrosis observed on [^{18}F]FDG PET and at immunohistochemistry it is likely to represent the reduction of tumor blood supply. At t2, we observed a slight difference between *in vivo* and *ex vivo* results. *In vivo*, the RGD SUVmax of the tumor was less in the BVZ-treated group than in the TMZ-treated group, without difference between TMZ + BVZ and the two other groups. But, *ex vivo*, the RGD % ID was significantly smaller in mice treated with TMZ + BVZ compared to the one treated with TMZ alone. This difference could be explained by the fact that the % ID is a more direct measurement than the SUVmax. The radiotracer uptake was determined on a ROI that may include other structures than the tumor, while the % ID includes only the tumor. It may thus be more sensitive to a decrease in integrin expression. The abundant angiogenesis in mice treated with TMZ was confirmed by the results of immunohistochemistry: the % MVD of the TMZ group was

heterogeneous, similar to that of the tumors of the control group (analyses were carried out on nonnecrotic zones) and statistically greater than those of the BVZ and TMZ + BVZ groups (Fig. 5). To the best of our knowledge, only the study of Xue et al. described similar results and found that TMZ could stimulate neovascularization 6 days after the start of treatment [40]. In our study, the evolution of tumor volume is not concordant with RGD uptake measurement, in bevacizumab treated groups. If evolution of tumor volume is considered to reflect antitumor effect, our results suggest that the [^{68}Ga]RGD allows the detection of the vascular antiangiogenic effects of bevacizumab but not its antitumor effect. [^{68}Ga]RGD PET was able to monitor the persistence of integrin expression in the TMZ-treated group at least similar to that of controls. This persistence was reflected neither by the evolution of tumor volume nor by tumor [^{18}F]FDG uptake.

Conclusions

[^{18}F]FDG PET visualized tumors but was not available to follow chemotherapy or antiangiogenic treatment in murine model tumor of U87MG human GB. In contrast, [^{68}Ga]RGD

appeared to be a useful PET agent for noninvasive imaging angiogenesis. The decrease in its tumor uptake as compared to controls reflected the effect of treatment with the antiangiogenic agent bevacizumab combined or not with temozolomide chemotherapy on tumor vasculature. In contrast, the treatment with temozolomide alone led to an increase in [⁶⁸Ga]RGD uptake.

Funding Information The study was supported by the French Association Nationale de la Recherche et de la Technologie (ANRT) and PETNET Solutions SAS, Siemens healthineers.

Compliance with Ethical Standards

Conflict of Interest

The authors declare that they have no conflict of interest.

References

- Carmeliet P, Jain RK (2000) Angiogenesis in cancer and other diseases. *Nature* 407:249–257
- Folkman J (1971) Tumor angiogenesis: therapeutic implications. *N Engl J Med* 285:1182–1186
- Folkman J (2007) Angiogenesis: an organizing principle for drug discovery? *Nat Rev Drug Discov* 6:273–286
- Folkman J (2007) Is angiogenesis an organizing principle in biology and medicine? *J Pediatr Surg* 42:1–11
- Ivy SP, Wick JY, Kaufman BM (2009) An overview of small-molecule inhibitors of VEGFR signaling. *Nat Rev Clin Oncol* 6:569–579
- Tarallo V, De Falco S (2015) The vascular endothelial growth factors and receptors family: up to now the only target for anti-angiogenesis therapy. *Int J Biochem Cell Biol* 64:185–189
- Bellou S, Pentheroudakis G, Murphy C, Fotsis T (2013) Anti-angiogenesis in cancer therapy: Hercules and hydra. *Cancer Lett* 338:219–228
- Sennino B, McDonald DM (2012) Controlling escape from angiogenesis inhibitors. *Nat Rev Cancer* 12:699–709
- Scott BJ, Quant EC, McNamara MB, Ryg PA, Batchelor TT, Wen PY (2010) Bevacizumab salvage therapy following progression in high-grade glioma patients treated with VEGF receptor tyrosine kinase inhibitors. *Neuro-Oncology* 12:603–607
- Ye W (2016) The complexity of translating anti-angiogenesis therapy from basic science to the clinic. *Dev Cell* 37:114–125
- Colavolpe C, Chinot O, Metellus P, Mancini J, Barrie M, Bequet-Boucard C, Tabouret E, Mundler O, Figarella-Branger D, Guedj E (2012) FDG-PET predicts survival in recurrent high-grade gliomas treated with bevacizumab and irinotecan. *Neuro-Oncology* 14:649–657
- Goggi JL, Bejot R, Moonshi SS, Bhakoo KK (2013) Stratification of ¹⁸F-labeled PET imaging agents for the assessment of antiangiogenic therapy responses in tumors. *J Nucl Med* 54:1630–1636
- Bao X, Wang MW, Luo JM, Wang SY, Zhang YP, Zhang YJ (2016) Optimization of early response monitoring and prediction of cancer antiangiogenesis therapy via noninvasive PET molecular imaging strategies of multifactorial bioparameters. *Theranostics* 6:2084–2098
- Corroyer-Dulmont A, Peres EA, Gerault AN, Savina A, Bouquet F, Divoux D, Toutain J, Ibazizène M, MacKenzie ET, Barré L, Bernaudin M, Petit E, Valable S (2016) Multimodal imaging based on MRI and PET reveals [¹⁸F]FLT PET as a specific and early indicator of treatment efficacy in a preclinical model of recurrent glioblastoma. *Eur J Nucl Med Mol Imaging* 43:682–694
- Sheldrake HM, Patterson LH (2009) Function and antagonism of beta3 integrins in the development of cancer therapy. *Curr Cancer Drug Targets* 9:519–540
- Desgrosellier JS, Cheresh DA (2010) Integrins in cancer: biological implications and therapeutic opportunities. *Nat Rev Cancer* 10:9–22
- Gaertner FC, Souvatzoglou M, Brix G, Beer AJ (2012) Imaging of hypoxia using PET and MRI. *Curr Pharm Biotechnol* 13:552–570
- Niu G, Chen X (2016) RGD PET: from lesion detection to therapy response monitoring. *J Nucl Med* 57:501–502
- Zhang H, Liu N, Gao S, Hu X, Zhao W, Tao R, Chen Z, Zheng J, Sun X, Xu L, Li W, Yu J, Yuan S (2016) Can an ¹⁸F-ALF-NOTA-PRGD2 PET/CT scan predict treatment sensitivity to concurrent chemoradiotherapy in patients with newly diagnosed glioblastoma? *J Nucl Med* 57:524–529
- Iagaru A, Mosci C, Mittra E, Zaharchuk G, Fischbein N, Harsh G, Li G, Nagpal S, Recht L, Gambhir SS (2015) Glioblastoma multiforme recurrence: an exploratory study of ¹⁸F FPPRGD2 PET/CT. *Radiology* 277:497–506
- Bozon-Petitprin A, Bacot S, Gauchez AS, Ahmadi M, Bourre JC, Marti-Batlle D, Perret P, Broisat A, Riou LM, Claron M, Boturyn D, Fagret D, Ghezzi C, Vuillez JP (2015) Targeted radionuclide therapy with RAFT-RGD radiolabelled with ⁹⁰Y or ¹⁷⁷Lu in a mouse model of $\alpha v \beta 3$ -expressing tumours. *Eur J Nucl Med Mol Imaging* 42:252–263
- Guo N, Zhang F, Zhang X, Guo J, Lang L, Kiesewetter DO, Niu G, Li Q, Chen X (2015) Quantitative evaluation of tumor early response to a vascular-disrupting agent with dynamic PET. *Mol Imaging Biol* 17:865–873
- Cui Y, Liu H, Liang S, Zhang C, Cheng W, Hai W, Yin B, Wang D (2016) The feasibility of ¹⁸F-AIF-NOTA-PRGD2 PET/CT for monitoring early response of Endostar antiangiogenic therapy in human nasopharyngeal carcinoma xenograft model compared with ¹⁸F-FDG. *Oncotarget* 7:27243–27254
- Kazmierczak PM, Todica A, Gildehaus FJ, Hirner-Eppeneder H, Brendel M, Eschbach RS, Hellmann M, Nikolaou K, Reiser MF, Wester HJ, Kropf S, Rominger A, Cyran CC (2016) ⁶⁸Ga-TRAP-(RGD)3 hybrid imaging for the in vivo monitoring of $\alpha v \beta 3$ -integrin expression as biomarker of anti-angiogenic therapy effects in experimental breast cancer. *PLoS One* 11:e0168248
- Rylova SN, Barnucz E, Fani M, Braun F, Werner M, Lassmann S, Maecke HR, Weber WA (2014) Does imaging $\alpha v \beta 3$ integrin expression with PET detect changes in angiogenesis during bevacizumab therapy? *J Nucl Med* 55:1878–1884
- Battle MR, Goggi JL, Allen L, Barnett J, Morrison MS (2011) Monitoring tumor response to antiangiogenic sunitinib therapy with ¹⁸F-fluciclatide, an ¹⁸F-labeled $\alpha v \beta 3$ -integrin and $\alpha v \beta 5$ -integrin imaging agent. *J Nucl Med* 52:424–430
- Eo JS, Jeong JM (2016) Angiogenesis imaging using ⁶⁸Ga-RGD PET/CT: therapeutic implications. *Semin Nucl Med* 46:419–427
- Haubner R, Maschauer S, Prante O (2014) PET radiopharmaceuticals for imaging integrin expression: tracers in clinical studies and recent developments. *Biomed Res Int* 2014:871609
- Knetsch PA, Petrik M, Griessinger CM, Rangger C, Fani M, Kesenheimer C, von Guggenberg E, Pichler BJ, Virgolini I, Decristoforo C, Haubner R (2011) [⁶⁸Ga]NODAGA-RGD for imaging $\alpha v \beta 3$ integrin expression. *Eur J Nucl Med Mol Imaging* 38:1303–1312
- Haubner R, Finkenstedt A, Stegmayr A, Rangger C, Decristoforo C, Zoller H, Virgolini IJ (2016) [⁶⁸Ga]NODAGA-RGD—metabolic stability, biodistribution, and dosimetry data from patients with hepatocellular carcinoma and liver cirrhosis. *Eur J Nucl Med Mol Imaging* 43:2005–2013
- Provost C, Prignon A, Rozenblum-Beddo L, Bruyer Q, Dumont S, Merabte F, Nataf V, Bouteiller C, Talbot JN (2018) Comparison and evaluation of two RGD peptides labelled with ⁶⁸Ga or ¹⁸F for PET imaging of angiogenesis in animal models of human glioblastoma or lung carcinoma. *Oncotarget* 9:19307–19316
- Frosina G (2016) Non-routine tracers for PET imaging of high-grade glioma. *Anticancer Res* 36:3253–3260
- Kreisl TN, Smith P, Sul J, Salgado C, Iwamoto FM, Shih JH, Fine HA (2013) Continuous daily sunitinib for recurrent glioblastoma. *J Neuro-Oncol* 111:41–48
- Corroyer-Dulmont A, Peres EA, Petit E et al (2013) Detection of glioblastoma response to temozolomide combined with bevacizumab based on muMRI and muPET imaging reveals [¹⁸F]-fluoro-L-thymidine as an early and robust predictive marker for treatment efficacy. *Neuro-Oncology* 15:41–56

35. Omuro A, Beal K, Gutin P, Karimi S, Correa DD, Kaley TJ, DeAngelis LM, Chan TA, Gavrilovic IT, Nolan C, Hormigo A, Lassman AB, Mellinger I, Grommes C, Reiner AS, Panageas KS, Baser RE, Tabar V, Pentsova E, Sanchez J, Barradas-Panchal R, Zhang J, Faivre G, Brennan CW, Abrey LE, Huse JT (2014) Phase II study of bevacizumab, temozolomide, and hypofractionated stereotactic radiotherapy for newly diagnosed glioblastoma. *Clin Cancer Res* 20:5023–5031
36. Huang J, Frischer JS, Serur A, Kadenhe A, Yokoi A, McCrudden KW, New T, O'Toole K, Zabski S, Rudge JS, Holash J, Yancopoulos GD, Yamashiro DJ, Kandel JJ (2003) Regression of established tumors and metastases by potent vascular endothelial growth factor blockade. *Proc Natl Acad Sci U S A* 100:7785–7790
37. Inai T, Mancuso M, Hashizume H, Baffert F, Haskell A, Baluk P, Hu-Lowe DD, Shalinsky DR, Thurston G, Yancopoulos GD, McDonald DM (2004) Inhibition of vascular endothelial growth factor (VEGF) signaling in cancer causes loss of endothelial fenestrations, regression of tumor vessels, and appearance of basement membrane ghosts. *Am J Pathol* 165:35–52
38. Beal K, Abrey LE, Gutin PH (2011) Antiangiogenic agents in the treatment of recurrent or newly diagnosed glioblastoma: analysis of single-agent and combined modality approaches. *Radiat Oncol* 6:2
39. Hombach-Klonisch S, Mehrpour M, Shojaei S, Harlos C, Pitz M, Hamai A, Siemianowicz K, Likus W, Wiechec E, Toyota BD, Hoshyar R, Seyfoori A, Sepehri Z, Ande SR, Khadem F, Akbari M, Gorman AM, Samali A, Klonisch T, Ghavami S (2018) Glioblastoma and chemoresistance to alkylating agents: involvement of apoptosis, autophagy, and unfolded protein response. *Pharmacol Ther* 184:13–41
40. Xue W, Du X, Wu H, Liu H, Xie T, Tong H, Chen X, Guo Y, Zhang W (2017) Aberrant glioblastoma neovascularization patterns and their correlation with DCE-MRI-derived parameters following temozolomide and bevacizumab treatment. *Sci Rep* 7:13894